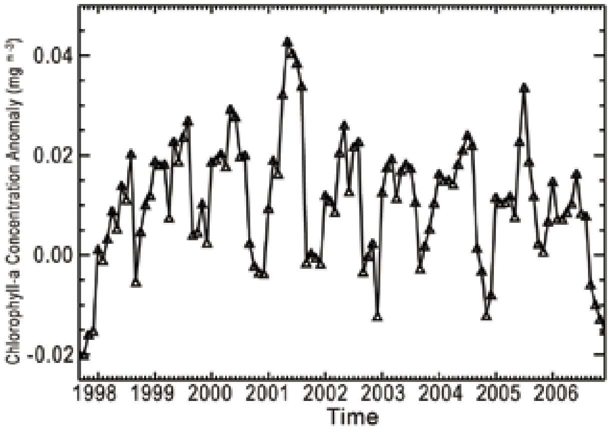

Fig. 3.21. Global area-averaged chlorophyll-a concentration anomalies (mg m^{-3}) for September 1997–December 2006.

ber 1997 through August 2006, and are mapped to an equidistant cylindrical projection with 9-km resolution at the equator. Each month is derived from nine years of monthly bins (online at http://reason.gsfc.nasa.gov/OPS/Giovanni/Readme_climate_seawifs.shtml).

Other anomalies to highlight are the above-normal chlorophyll concentration of approximately 0.043 mg m^{-3} in May 2001 and below-normal concentration of approximately −0.02 mg m^{-3} in the boreal fall of 1997 (Fig. 3.21). The below-normal concentrations in 1997 are a direct result of the extremely strong 1997/98 El Niño event. The peak in May 2001 is attributed to the negative state of the NAO. When the NAO index is negative, phytoplankton biomass and productivity in the North Atlantic have higher-than-mean conditions because of enhanced winter mixing of subtropical waters (Yoder and Kennelly 2003; Follows and Dutkiewicz 2002).

El Niño and La Niña events alter the previously described seasonal cycle of phytoplankton stocks in the Northern Hemisphere. Peak concentrations are observed during boreal summer in La Niña events and minimal concentrations occur during boreal fall in El Niño events. Several studies have been conducted in regard to the central/eastern equatorial Pacific chlorophyll decrease during the 1997/98 El Niño and the increase during the subsequent La Niña (Murtugudde et al. 1999; Chavez et al. 1998, 1999; Wilson and Adamec 2001; Ryan et al. 2002). Each of these studies illustrate that during a La Niña event, trade wind intensification prompts thermocline and nutricline shoaling, which increases the nutrient flux to the surface layer, generating intense phytoplankton blooms; conversely, during an El Niño event the thermocline and nutricline deepen, which impinges upwelling and reduces the supply of nutrients into the euphotic zone, thereby limiting chlorophyll production.

The year 2006 marked the beginning of the 2006/07 El Niño event. Both the 1997/98 and 2002/03 El Niños exhibited their lowest chlorophyll concentrations during the month of December. For the 2006/07 El Niño it is yet to be known at the time of writing whether peak below-normal concentrations do in fact occur in December. However, it is safe to say, based upon the available chlorophyll data, that the 2006/07 El Niño is stronger (in terms of its effects on chlorophyll) than the 2002/03 El Niño (with a below-normal concentration of approximately −0.031 mg m^{-3} in December 2006 in the Niño 3.4-region compared to approximately −0.024 mg m^{-3} in December 2002), but is less intense than the strong El Niño of 1997/98, which had a below-normal concentration of approximately −0.09 mg m^{-3} in December 1997 in the Niño 3.4-region.

4. THE TROPICS—H. J. Diamond

a. Overview—H. J. Diamond

This Tropics section consists of global input on the following three primary topics: 1) ENSO and the tropical Pacific, 2) TC activity for the 2006 season in seven basins (the Atlantic, northeast Pacific, northwest Pacific, North and South Indian, South Pacific, and Australia), and 3) ITCZ behavior in the Pacific and Atlantic basins.

The year was characterized by a transition from La Niña conditions in the first quarter of the year to El Niño conditions during the last quarter of the year. Regarding TC activity, the 2006 Atlantic season was much different than the 2005 season as follows: the number of storms dropped from 28 in 2005 to 10 in 2006, the northeast Pacific was a bit more active than in 2005, and the Australian basin had several strong storms.

b. ENSO and the tropical Pacific—G. D. Bell and M. S. Halpert

1) Overview

El Niño and La Niña episodes represent opposite phases of ENSO. These episodes are often defined from a time series of area-averaged SST anomalies in the Niño-3.4 region (called the Niño-3.4 index), which spans the central and east-central equatorial Pacific between 5°N–5°S and 170°–120°W. During 2006, this index showed below-average SSTs associated with La Niña during January–March, followed by a return to near-average temperatures and ENSO-neutral conditions during April–July (Fig. 4.1).

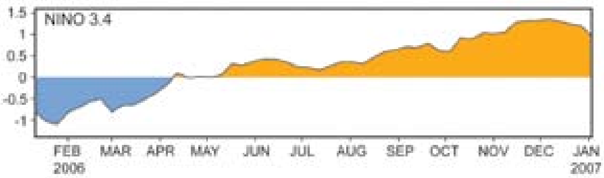

Fig. 4.1. Time series of the Niño-3.4 region SST anomaly index.

El Niño conditions developed during August and September, with Niño-3.4 temperatures increasing to more than +1.2°C above average during November and December.

The surface and subsurface temperature anomaly patterns show the changes across the central and east-central equatorial Pacific during 2006 (Fig. 4.2). Between December–February 2005/06 and September–November 2006, anomalies warmed 2°–3°C across much of the region (Figs. 4.2a,b), and subsurface temperature anomalies warmed 3°–6°C (Figs. 4.2c,d). This warming is associated with increased depths of the 20°C isotherm (thick black line), which approximates the center of the oceanic thermocline.

The strong coupling between surface and subsurface temperature anomalies is a well-known characteristic of both El Niño and La Niña, and reflects their link to changes in thermocline depth (Figs. 4.3a,b). During La Niña, stronger-than-average tropical easterly winds in the lower atmosphere produce increased upwelling, which leads to shallower thermocline depths and cooler ocean temperatures. Conversely, weaker-than-average tropical easterlies during El Niño result in decreased upwelling, which leads to increased thermocline depths and warmer waters. The transition from La Niña to El Niño during 2006 was indeed accompanied by a significant weakening of the 850-hPa equatorial easterlies, which were stronger than average early in the year (blue shading) and generally weaker than average after May (orange shading, Fig. 4.3c).

The development of El Niño also followed a sharp transition in the overall distribution of anomalous convection during May and June across the equatorial Pacific (Fig. 4.4). This transition mainly featured a westward shift in the area of suppressed convection (brown shading) from the date line to the western Pacific. However, enhanced convection near the date line did not become established until mid-September, which coincided with a significant warming of the central and east-central equatorial Pacific. This anomalous tropical convection led to several well-known El Niño impacts, including 1) below-average rains across northeastern Australia, Indonesia, and the western tropical Pacific, 2) fewer Atlantic hurricanes and more East Pacific hurricanes than in recent years, 3) above-average temperatures across the northern half of the United States during November–December, and 4) stormier- and wetter-than-average conditions across the southeastern United States during November–December.

2) The MJO and Kelvin wave activity

Low-frequency variability in the Tropics is strongly influenced by the MJO (Madden and Julian 1971, 1972, 1994), a tropical disturbance that modulates tropical convection and atmospheric circulation patterns with a typical period of 30–60 days. The MJO tends to be most active during ENSO-neutral years, and can produce ENSO-like anomalies (Mo and Kousky 1993; Kousky and Kayano 1994). The low- (850 hPa) and upper- (200 hPa) level equatorial zonal winds, tropical convection, and both sea surface and subsurface temperature anomalies exhibited considerable intraseasonal variability during 2006 in association with the MJO.

The MJO is indicated in a

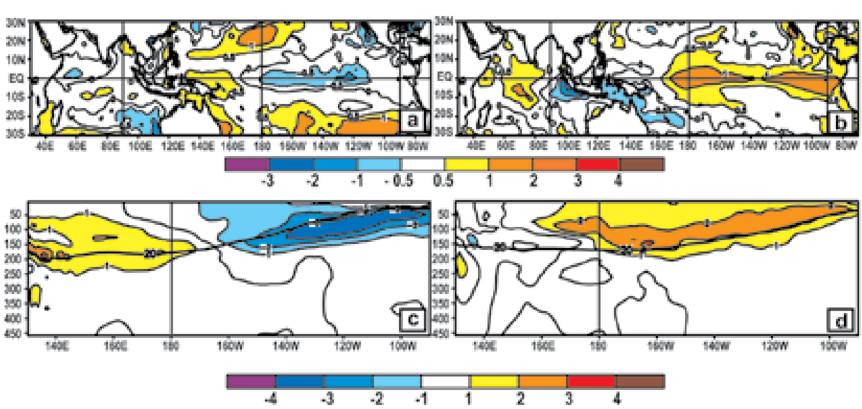

Fig. 4.2. Seasonal SST anomalies (top) and depth–longitude section of subsurface temperature anomalies (bottom) for (a), (c) DJF 2005/06 and (b), (d) SON 2006. The 20°C isotherm (thick black line) is also plotted in panels (c), (d). SST anomalies are departures from the 1971–2000 adjusted OI climatology (Smith and Reynolds 1998). The subsurface analysis is based on data derived from an analysis system that assimilates oceanic observations into an oceanic GCM (Behringer et al. 1998), and anomalies are departures from the 1981–2000 base period means.

time–longitude section by continuous propagation of the 200-hPa velocity potential anomalies around the globe (Fig. 4.5). During April–December, several periods of MJO-related suppressed convection (brown shading, see Fig. 4.4) and anomalously weak low-level tropical easterly winds were evident over the western tropical Pacific. These conditions can initiate oceanic equatorial Kelvin waves, which are eastward-propagating gravity waves featuring downwelling in the mixed layer at their leading edge and upwelling in their wake (Zhang et al. 2001). A typical eastward propagation rate for these waves is roughly 10° of longitude per week.

Four major Kelvin waves occurred during April–December, with the amplitude of each wave exceeding that of its predecessor. Prior to and during El Niño's development, these waves acted to significantly modulate the upper-ocean heat content across the central and east-central equatorial Pacific. The warming associated with the downwelling phase of a particularly strong Kelvin wave during September prompted NOAA to report that El Niño had developed. This was followed during November and December by an even stronger Kelvin wave and additional warming.

c. *Tropical cyclones*

1) Seasonal activity overview—H. J. Diamond and D. H. Levinson

Averaged across all basins, the tropical storm season of 2006 (2005/06 in the Southern Hemisphere) had a below-normal (1981–2000 base) number of tropical storms, fewer HTC, but a greater number of major HTCs than average. Globally, 78 TS (> 33 kt) were recorded, with 42 becoming HTCs, and of these 26 attained major/intense (> 95 kt) status (compared to an average of 97, 55, and 25 storms, respectively). While 2005 was a more active season overall, the number of major HTCs in both 2005 (28) and 2006 (26) were similar.

The 2006 season was near average in three basins (Atlantic, North Indian, and southwest Pacific), slightly above average in two basins (northeast Pacific and Australian), and slightly below average in two basins (northwest Pacific and South Indian). As a result of El Niño conditions described earlier in the section, the Atlantic season was notable (e.g., no landfalling hurricanes in the United States versus seven in 2005). The highlight of the Australian sea-

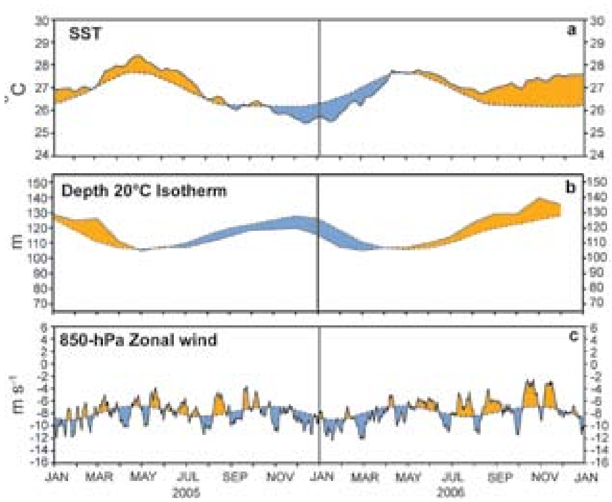

Fig. 4.3. Monthly time series of (a) SST (°C), (b) the depth of the 20°C isotherm (m), and (c) 850-hPa zonal wind speed (m s^{-1}), over the central and east-central equatorial Pacific. Values were averaged over the region bounded by 5°N–5°S and 180°–100°W. Five-day and (solid line) climatological values (1979–95; dashed line) are shown, as are positive (orange) and negative (blue) anomalies relative to the 1979–95 base period.

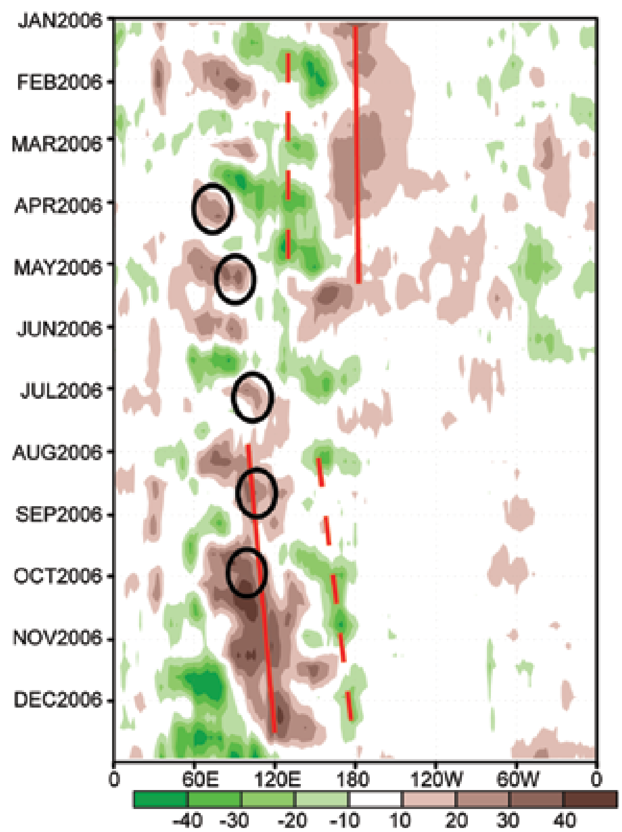

Fig. 4.4. Time–longitude section of OLR anomalies (W m^{-2}) during 2006. Solid (dashed) red lines indicate main areas of suppressed (enhanced) convection. Black circles indicate suppressed convection associated with initiation of equatorial oceanic Kelvin waves. Anomalies are based on 5-day average values, and are departures from the 1979–95 base period pentad means. A 1–2–1 smoother was applied to the data.

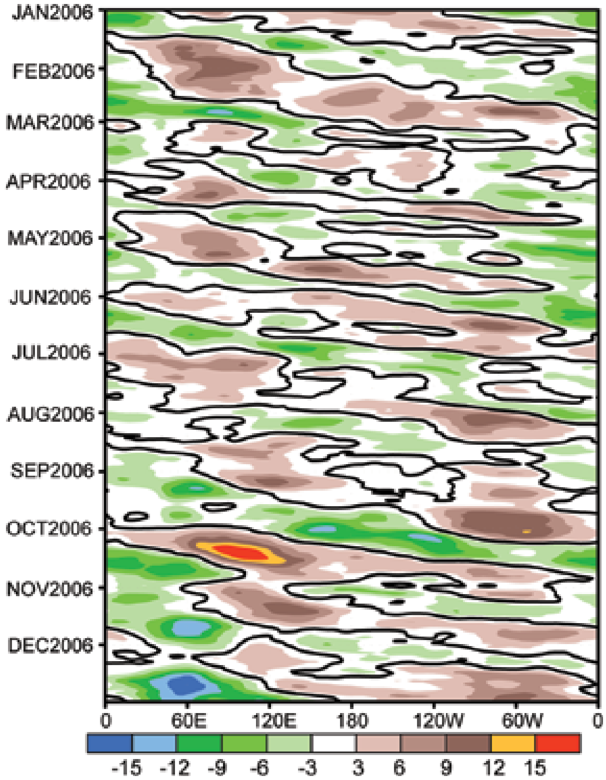

Fig. 4.5 Time–longitude section (5°N–5°S) of daily 200-hPa velocity potential anomalies during 2006. The shading interval is 3×10^6 m^2 s^{-1}, and the thick solid contour is the zero line. Green (brown) shading is indicative of anomalous upper-level divergence (convergence). Anomalies are departures from the 1971–2000 base period daily means, and are plotted using a 5-day running-mean smoother.

son was the occurrence of three Australian category 5 storms (Fig. 4.6), one of which was the strongest TC in Queensland since 1918, and one that was the strongest TC ever observed in the Northern Territory (see sidebar: An Australian Season of Extremes: Yes, We Have No Bananas).

2) Atlantic basin—G. D. Bell, E. Blake, C. W. Landsea, M. Chelliah, R. Pasch, K. C. Mo, and S. B. Goldenberg

The 2006 Atlantic hurricane season produced 10 TSs, five Hs, and two MHs [categories 3–5 on the Saffir–Simpson scale (Simpson 1974)]. These values are slightly below the 1950–2000 averages of 11 TSs, 6 Hs, and 2.5 MHs.

A widely used measure of seasonal activity is NOAA's ACE Index (Bell et al. 2000). The ACE Index accounts for the combined strength and duration of TCs during the season. The 2006 ACE Index was 90% of the 1950–2000 median value (87.5×10^4 kt^2), indicating a near-normal season (Fig. 4.7). This value

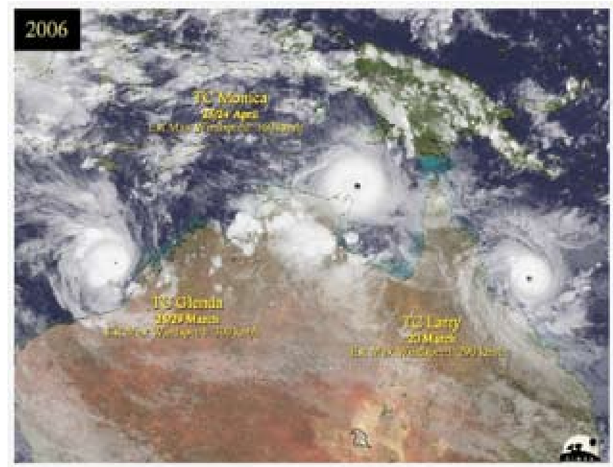

Fig. 4.6. Satellite montage of Australian category 5 landfalling tropical cyclones. [Source: C. Velden, University of Wisconsin—Madison, CIMSS.]

is well below the three previous seasons, which averaged 247% (Bell et al. 2005) and less than one-third of the record high (284%) seen in 2005 (Bell et al. 2006).

The reduced activity during 2006 reflects the competing influences of two dominant climate factors. The first dominant factor is El Niño, which suppressed activity during September and October through anomalous upper-level convergence and sinking motion across the Caribbean Sea. Anomalous circulation features not related to El Niño accentuated this signal at times, and also contributed to the reduced activity. The second dominant climate factor was the set of ongoing oceanic and atmospheric conditions that have been conducive to above-normal hurricane seasons since 1995, which remained strong during the climatological peak months ASO of the season.

El Niño's suppressing influence on Atlantic hurricane activity is well documented (Gray 1984; Tang and Neelin 2004; Bell and Chelliah 2006), and is clearly evident during the current active hurricane era that began in 1995. During 1995–2006, 9 of 12 hurricane seasons were in the above-normal tercile, defined as ACE larger than 117% of the median. The three exceptions are all El Niño years (1997, 2002, and 2006).

The large-scale El Niño signal during ASO 2006 is evident in the patterns of anomalous 200-hPa velocity potential and streamfunction. In the Tropics velocity potential anomalies are related to the upper-level divergent circulation and anomalous convection. Negative velocity potential anomalies across the central and east-central equatorial Pacific reflect the

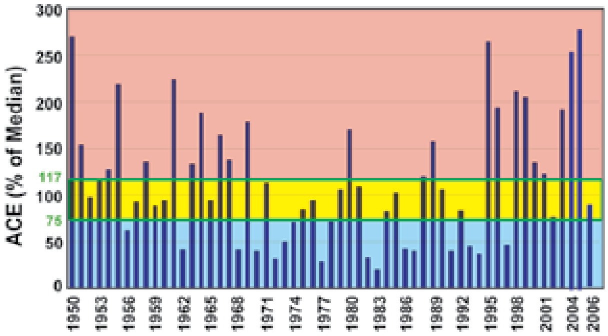

FIG. 4.7. NOAA's ACE Index expressed as percent of the 1951–2000 median value (87.5×10^4 kt^2). ACE is a wind energy index, and is calculated by summing the squares of the 6-hourly maximum sustained wind speed in knots (Vmax^2) for all periods while the system is a tropical storm, subtropical storm, or hurricane. Season types are indicated by the background shading, with pink, yellow, and blue indicating NOAA's classifications for above-, near-, and below-normal seasons, respectively.

El Niño–related enhanced convection and anomalous upper-level divergence. Positive values over both the western Pacific/Indonesia region and the Caribbean Sea reflect compensating anomalous upper-level convergence and suppressed convection. Another characteristic El Niño signature is anomalous upper-level ridges (positive streamfunction anomalies in the NH, and negative streamfunction anomalies in the SH) in the subtropics of both hemispheres flanking the region of enhanced convection over the central equatorial Pacific. However, this feature was not evident until October.

El Niño's typical impacts over the western tropical Atlantic Ocean and Caribbean Sea include increased vertical wind shear between 200 and 850 hPa and anomalous sinking motion in the middle and upper atmosphere. During ASO 2006, El Niño appears to have suppressed TC activity mainly by contributing to anomalous upper-level convergence and sinking motion across the Caribbean Sea. This suppressing influence was particularly notable during September and October, when only one TC developed over the Caribbean Sea despite low wind shear (< 8 m s^{-1}) (Fig. 4.8a) and anomalously warm SST. During September, the same conditions, but with no anomalous sinking motion, led to the formation of several hurricanes and major hurricanes over the central and eastern tropical Atlantic Ocean.

SST anomalies during ASO were positive throughout the North Atlantic (Fig. 4.9a). For the entire MDR, which encompasses the tropical Atlantic Ocean and Caribbean Sea (Goldenberg and Shapiro 1996), area-averaged SSTs during ASO were 0.68°C above average, the second warmest in the historical record dating back to 1871 (Fig. 4.9b). The reduced activity despite this anomalous warmth is consistent with previous findings, indicating that local atmospheric circulation anomalies, rather than local SST anomalies, are the dominant contributor to seasonal fluctuations in Atlantic hurricane activity (Shapiro and Goldenberg 1998; Bell and Chelliah 2006).

The vertical wind shear pattern during ASO 2006 primarily reflected anomalously weak shear (relative to the period 1971–2000) throughout the MDR in association with the ongoing active hurricane era (Fig. 4.8a). A modest El Niño–related increase in wind shear was evident over the western Caribbean Sea, but only when the departures are calculated relative to the current active era (Fig. 4.8b).

As with the 200-hPa streamfunction anomalies, there is little indication that El Niño affected the vertical wind shear prior to October. Even then, there is little evidence that the increased shear contributed to the shutdown in activity. For example, the main suppressing influence from strong vertical shear (> 8 m s^{-1}) occurred in August, prior to the time when El Niño began affecting this field. During September and October, the shear was quite weak across the Caribbean Sea, and was, therefore, not a

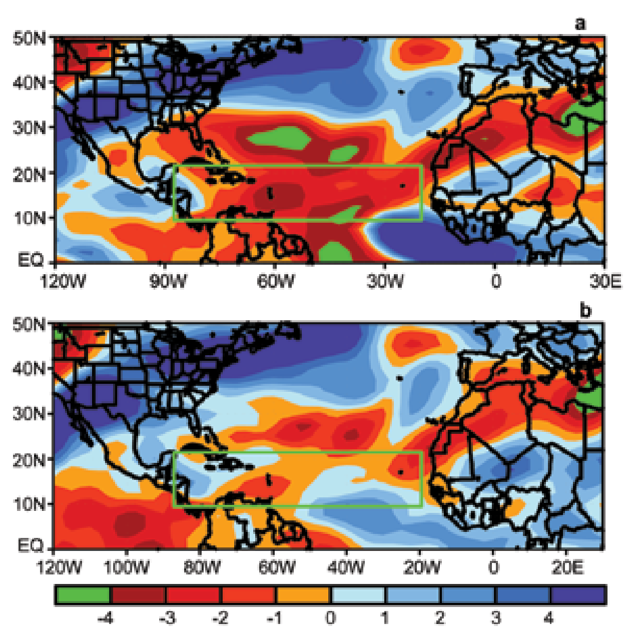

FIG. 4.8. August–October 2006: Anomalous strength of the total 200–850 hPa vertical wind shear, calculated with respect to (a) the 1971–2000 and (b) the 1995–2005 period monthly means. Red shading indicates below-average strength of the vertical shear. Green box denotes the main development region.

suppressing factor.

Although El Niño appears to be the primary cause for the reduced TC activity, highly variable circulation features not linked to El Niño also helped to suppress the activity. For example, during August increased vertical wind shear associated with an enhanced midoceanic trough led to reduced activity across the central MDR. During September, a deep trough near the U.S. east coast contributed to an anomalous sinking motion over the Gulf of Mexico. During October, an enhanced upper-level ridge over the south-central United States and western Gulf of Mexico contributed to the anomalous sinking motion over the Gulf of Mexico and accentuated the sinking motion over the Caribbean Sea. These conditions resulted in the third earliest end (following 1983 and 1993) to seasonal activity since routine daily satellite coverage began in 1966.

It is not clear why the El Niño signal was manifested mainly in the upper-level divergence and vertical motion fields, as opposed to the 200–850-hPa vertical wind shear, as is typical for most episodes. Also, while it is possible that the MJO (see section 4bii) may have accentuated the vertical motion patterns (e.g., Mo 2000), no such influence was evident during August and September. However, it is possible that the strong MJO signal in October contributed to the suppressed convection and lack of TC activity across the western Caribbean Sea in that month.

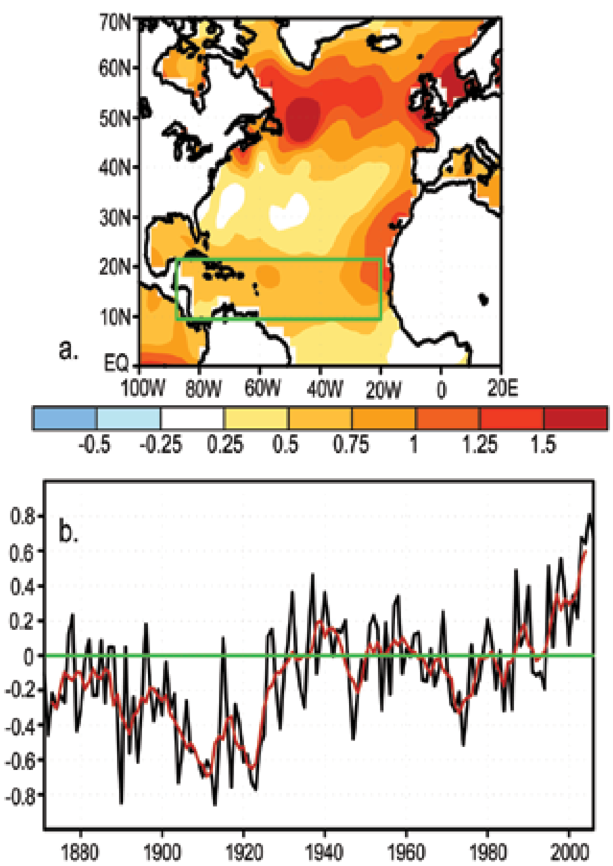

Fig. 4.9. (a) SST anomalies (°C) during August–October 2006, and (b) time series of area-averaged SST anomalies for the main development region [green boxed region shown in (a)]. Red line in (b) shows the corresponding 5-yr running mean. Anomalies are departures from the 1971–2000 period monthly means.

Only three Atlantic tropical storms—Alberto, Beryl, and Ernesto—struck the continental United States during 2006. Also, this was the first year since 2001 that no hurricanes struck the continental United States. This represents a sharp drop in strikes compared to the preceding four years (2002–05), when an average of seven named storms and three hurricanes per season struck the continental United States. In September (four of the five 2006 hurricanes formed in September), the deep trough near the U.S. east coast was critical in steering hurricanes out to sea long before they reached the coast. The overall suppression of activity over the western part of the Atlantic basin, in part resulting from El Niño, also contributed to fewer U.S. strikes.

Despite the reduced activity, key oceanic and atmospheric features continued to reflect the ongoing active Atlantic hurricane era. A main contributing factor to this active era is the tropical multidecadal signal, which reflects the leading modes of tropical convective rainfall variability occurring on multidecadal time scales (Bell and Chelliah 2006). The ongoing warm phase of the Atlantic multidecadal mode (Goldenberg et al. 2001), indicated by a continuation of above-average SSTs in the North Atlantic (Fig. 4.9b), is one important aspect of the tropical multidecadal signal. Some of this persistent anomalous warmth has also been linked to increasing global temperatures over the last 100 years (Santer et al. 2006).

Other very important and interrelated aspects of the tropical multidecadal signal and the ongoing active hurricane era that were also in place during 2006 included 1) an enhanced West African monsoon system (Landsea and Gray 1992) and suppressed convection in the Amazon basin, 2) enhanced upper-level ridges in both hemispheres over the Atlantic Ocean, 3) reduced wind shear across the tropical Atlantic (Fig. 4.10a), 4) an enhanced tropical easterly jet at 200 hPa and reduced tropical easterlies at 700 hPa across the tropical Atlantic (Fig. 4.10b), and 5) increased cyclonic relative vorticity across the eastern MDR (Fig. 4.10c). In light of these conditions, there is no indication that the current active hurricane era has ended. Instead, the El Niño–related reduction in activity merely represents a short-term break (similar to the 1997 and 2002 El Niño years) in an ongoing string of active hurricane seasons that began in 1995.

3) East Pacific basin—D. H. Levinson

(i) Overview of the 2006 season

The hurricane season in the ENP basin officially begins on 15 May and continues through the end of November, with peak activity occurring in September. The ENP basin includes two subregions officially used by NOAA/NWS to issue warnings: the east Pacific warning area extends from the western coast of North America to 140°W, which is the responsibility of NOAA's National Hurricane Center in Miami, Florida, while the region between 140°W to the date line is the responsibility of NOAA/Central Pacific Hurricane Center collocated at the NWS Weather Forecast Office in Honolulu, Hawaii.

In 2006, the hurricane season in the ENP was above normal, with a total of 18 NSs, 10 Hs, and 6 MHs having developed in the basin, which was above the 1971–2000 climatology of 16.4 NSs, 9.6 Hs, and 4.8 MHs each year. In terms of landfalling TCs, the 2006 season was also above average with two hurricanes making landfall along the Pacific coast of Mexico, and one of these as a major hurricane. Over the period 1951–2000, 1.34 TSs, 1.3 Hs, and 0.3 MHs annually made landfall along Mexico's Pacific coast each year (Jauregui 2003).

(ii) Comparison of the 2006 season with climatology

Seasonal activity in 2006 was above normal compared with the climatological mean for the majority of indices. Figure 4.11 shows the seasonal variability of TC activity in the ENP basin covering the period 1970–2006. In terms of the number of NSs, which is

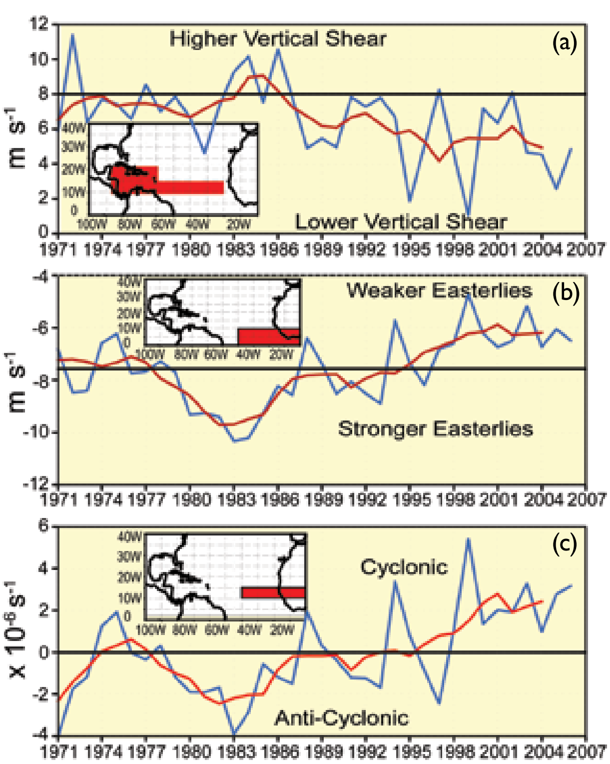

Fig. 4.10. August–October seasonal time series showing area-averaged values for key regions of (a) magnitude of the 200–850-hPa vertical shear of the zonal wind (m s^{-1}), (b) 700-hPa zonal wind (m s^{-1}), and (c) 700-hPa relative vorticity (x 10^{-6} s^{-1}). Blue curve shows unsmoothed 3-month values, and red curve shows a 5-point running mean of the time series. Averaging regions are shown in the insets.

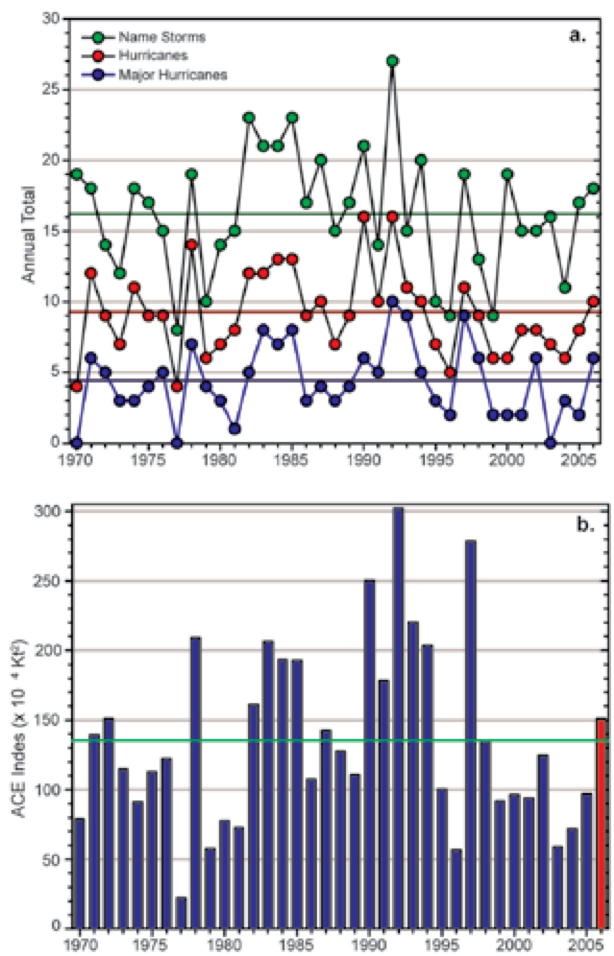

Fig. 4.11. Seasonal tropical cyclone statistics for the east North Pacific Ocean over the period 1970–2006: (a) number of NSs, Hs, and MHs and (b) the ACE Index (x 10^4 kt^2) with the seasonal total for 2006 highlighted in red. Both time series include the corresponding 1971–2000 base period means.

the total number of TCs that reached at least minimal tropical storm strength (sustained winds ≥ 34 kt), activity in the ENP basin has been near average since the mid-1990s, fluctuating between slightly above or below the long-term mean each year (Fig. 4.11a). However, in terms of H and MH, most seasons have been below normal since the mid-1990s. In fact, since 1995 NOAA has identified 7 of the 12 ENP seasons as being below normal, and only the 1997 and 2006 El Niño–influenced seasons as being above normal. This is in sharp contrast to higher activity seen during the preceding 1970–94 period, when only 6 of 24 (25%) hurricane seasons were below normal and 9 of 24 (38%) were above normal.

The ACE Index (Bell et al. 2000; Bell and Chelliah 2006) value for the ENP basin in 2006 was 150.68×10^4 kt^2, which was above both the long-term mean and median, and also at the upper end of NOAA's definition of a "near normal" season. Prior to the above-normal 2006 season, there had been a marked decrease in the ACE Index for the ENP basin beginning in 1995, with the only exception being the aforementioned 1997 hurricane season that corresponded with the last strong El Niño event in the Pacific Ocean. Another interesting aspect of the below-normal activity in the ENP since 1995 has been the inverse relationship to the observed increase in activity in the North Atlantic basin (Lander and Guard 1998), and the so-called Atlantic multidecadal mode (Landsea et al. 1998, 1999; Goldenberg et al. 2001; Bell and Chelliah 2006). Both the maximum wind speed and the mean maximum wind speed have had a slight decreasing trend in the last decade. More obvious has been the decrease in mean hurricane duration in the ENP basin, which was ~3.9 days in 2006, slightly below the 4–5 days during the most active years. The recent decade of low activity reached a minimum in 2003, and since that time there has been an increase in all indicators over the past three seasons.

In terms of the timing of activity in the ENP basin, the 2006 season was unusually slow to develop. After the formation of TS Aletta in late May, no named storms formed in June, which previously had only occurred once before (in 2004) during the period of reliable data. The below-normal activity continued into early July, because there were no TCs during the first half of the month; but, cyclogenesis increased dramatically during the second half of July as three hurricanes (MH Bud, H Carlotta, and MH Daniel) and one tropical storm (TS Emilia) developed. Above-normal activity persisted into August, with five hurricanes, three of which reached major hurricane strength (Ioke, Ileana, and John). Of note, MH Ioke, which officially developed in the central Pacific warning area, reached category 5 intensity and propagated westward past the date line into the West Pacific basin, becoming a super-TY during its life cycle. In September, one hurricane (Lane) and one tropical storm (Miriam) formed, as overall activity to this point of the season was near normal. However, both October and November were above average. Three named storms developed during October (TS Norman, TS Olivia, and H Paul), which normally has only two (on average 1 TS and 1 H), while November 2006 was the most active in the reliable historical record. Two named storms formed during the month (TS Rosa and H Sergio), and only in 1966 had there previously been two tropical storms during any November on record. The final TC of the season, H Sergio, was the most intense hurricane ever observed in November (category 2; maximum sustained winds ~95 kt) in the ENP basin, and it was also the longest-lived TC for the month, with a record 5.5 days at tropical storm strength or greater.

(iii) Environmental influences on the 2006 eastern North Pacific hurricane season

Previous studies have demonstrated that TC activity (both frequency and intensity) in the ENP basin is directly influenced by several large-scale environmental factors, including SSTs, vertical wind shear in the mid- and upper troposphere, the phase of the QBO in the tropical lower stratosphere, and the phase of ENSO in the equatorial Pacific region (Whitney and Hobgood 1997).

In 2006, above-normal vertical wind shear in the midtroposphere (200–850 hPa) was observed in the ENP basin during the first half of the season (June–August; see Fig. 4.12). Vertical wind shear anomalies exceeding 9 m s^{-1} occurred in the ENP basin's MDR, which is the area between 10°–20°N and 90°–130°W off the coast of Mexico (green box in Fig. 4.12). Three-month-averaged wind shear anomalies exceeding 12 m s^{-1} were also measured west of the Baja Peninsula. In addition to the increased vertical wind shear, the SSTs were near normal in the MDR during June and July, while warmer SSTs developed in August when an area from +0.5° to +1.0°C SST anomalies developed off the coast of the Baja Peninsula (Fig. 4.13). The situation changed dramatically during the latter half of the season, as the moderate El Niño formed in September; the midtropospheric wind shear anomalies weakened and SSTs increased in response to the developing warm event. As a result, warmer-than-normal SST anomalies persisted over the eastern half of the MDR during September and

October (Fig. 4.13).

Variability of the tropical atmosphere on interannual time scales related to ENSO and the QBO has been shown to modulate seasonal activity, affecting both the intensity and frequency of TCs in the ENP basin (Whitney and Hobgood 1997). According to NOAA/National Hurricane Center, above-normal TC activity in the ENP basin typically occurs during El Niño years, while seasons with ENSO-neutral conditions tend to have less activity, and seasons with the lowest activity are typically associated with La Niña years. In contrast, utilizing data covering the period 1963–93, Whitney and Hobgood (1997) found only a marginal relationship between ENSO phase and ENP activity, although their results showed that TCs in El Niño years reach their maximum intensities slightly farther south and west than during non–El Niño years. Obviously, the strength and timing of the SST anomalies associated with ENSO warm events is an important aspect to this relationship. The moderate 2006/07 El Niño event developed during late August and early September, so the phase of ENSO was transitioning from a neutral to a warm event during the peak of the hurricane season, and was the major factor influencing the above-normal season in 2006.

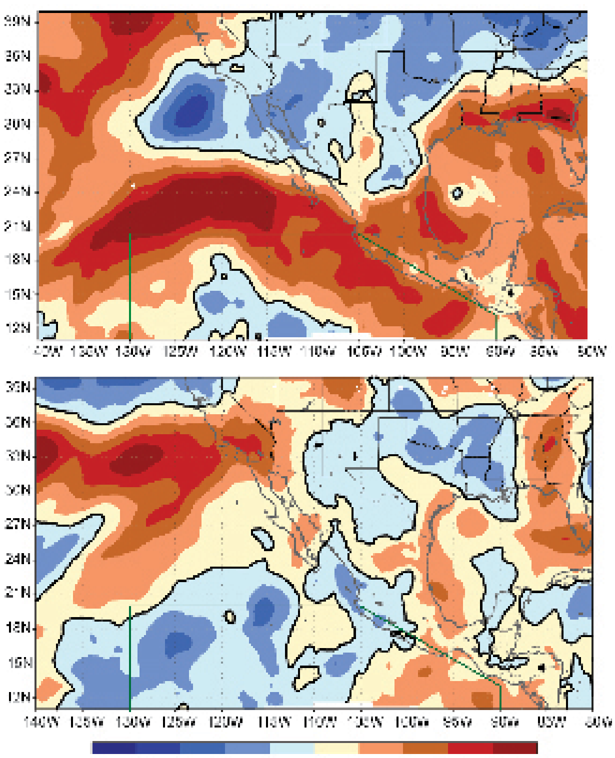

Fig. 4.12. The 200–850 hPa vertical wind shear anomaly (m s^{-1}) averaged over the following periods: (top) June–August and (bottom) September–November 2006. The main development region for ENP hurricanes is the area delineated by the green polygon in both maps. [Source: NOAA NOMADS, NARR dataset, with anomalies determined relative to the 1979–2004 base period mean.]

(iv) Impacts in 2006

There were no landfalling tropical systems in the ENP during the first half of the season, although four systems impacted the Mexican coast (TS Aletta, TD 02E, H Daniel, and TS Emilia). Above-normal activity during the second half of the season in the ENP basin resulted in two landfalling hurricanes and rainfall impacts from the remnants of tropical storms.

The first landfalling hurricane of the season was MH John, which reached category 4 intensity before weakening and eventually making landfall at category 2 strength in southern Baja ~65 km northeast of Cabo San Lucas early on 2 September. John generated numerous impacts, including 280 mm of rain at San Jose de los Planes near the landfall location, the overflow of the Iguagil Dam in Comundu, coastal flooding in the Acapulco area, and an official total of five deaths directly attributed to the storm. Major Hurricane Lane came ashore at category 3 intensity with winds ~110 kt along the Peninsula de Guevedo in Sinaloa. Lane interacted with the coastal moun-

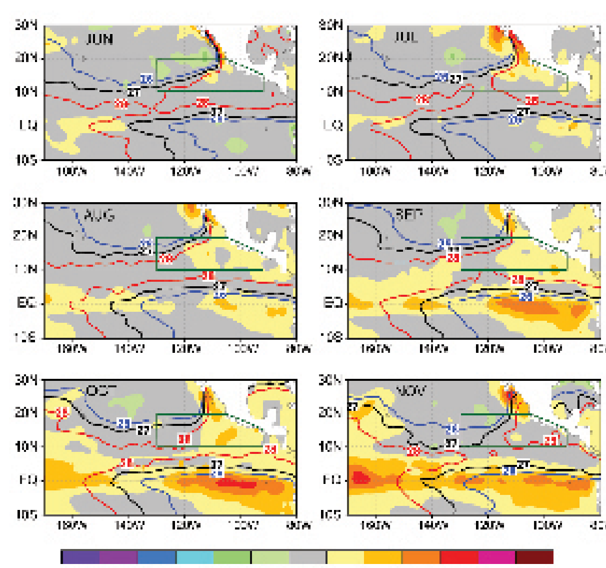

Fig. 4.13. Monthly averaged SSTs calculated using NOAA's OI dataset (Reynolds and Smith 1994; Reynolds et al. 2002). Isotherms denote monthly averaged SSTs and shading represents SST anomalies (°C) for each month (June–November) of the hurricane season in 2006. The MDR for ENP hurricanes is the area delineated by the green polygon in each plot.

tains, producing heavy rainfall, flooding, and mudslides over many areas along the Pacific Coast, with four fatalities directly attributed to this landfall. Hurricane Paul, which reached category 2 intensity on 23 October, resulted in four deaths associated with flooding.

4) Western North Pacific basin—S. J. Camargo

In 2006, a total of 27 TCs (including 3 TDs) occurred in the western North Pacific. This was below the climatological (1970–2004) median of 31, matching the 25th percentile of the climatological distribution. In Fig. 4.14a the number of TSs, TYs, and super-TYs per year is shown. There were 24 TCs reaching TS intensity or higher, according to the JTWC preliminary reports, but two of them were not named (01W and 17W). The climatological median for NSs: TSs and TYs is 26; 24 NSs also match the 25th percentile of the climatological distribution. There were 15 TYs in 2006, which is slightly below the climatological median of 16. In contrast, the number of super-TYs in 2006 (7) was in the top quartile of the climatological distribution (median is four, 75th percentile is five). A high number of intense TYs is typical during El Niño years in the western North Pacific (Camargo and Sobel 2005). Since 1970, when the data are more reliable, only two other years had more super-TYs than in 2006, and they occurred in 1997 and 2002, both of which were El Niño years. Another typical characteristic of El Niño years is an above-normal occurrence of central Pacific hurricanes (Chu and Wang 1997; Clark and Chu 2002), with some of the central Pacific hurricanes moving into the western North Pacific, as was the case with H/super-TY Ioke in 2006.

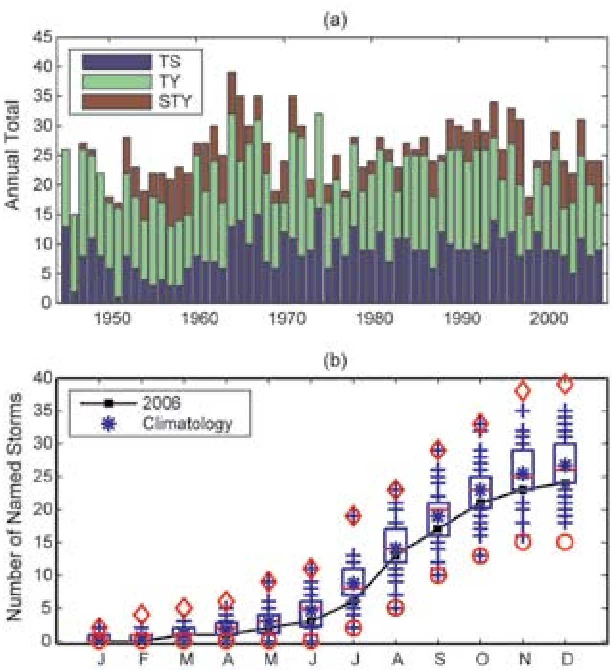

Fig. 4.14. (a) Number of tropical storms, typhoons, and supertyphoons per year in the western North Pacific for the period 1945–2005. (b) Cumulative number of tropical storms with tropical storm intensity or higher per month in the western North Pacific: 2006 (black squares and line), and climatology (1970–2004) shown as box plots [interquartile range: box, median: red line, mean: blue asterisk, values in the top or bottom quartile: blue crosses, high (low) records in the 1945–2005 period: red diamonds (circles)]. [Source: 1945–2004 JTWC best-track dataset, 2005/06 JTWC preliminary operational track data.]

The cumulative number of TCs per month climatologically and in 2006 are shown in Fig. 4.14b. The 2006 western North Pacific TC season started slowly in March with a TC that reached TS intensity (01W), but was given no name. The next TC (Chanchu) occurred in May and reached super-TY (≥ 130 kt maximum sustained winds) intensity. Tropical cyclone activity continued to be below normal in June and July, with one and three TCs, respectively, placing that period in the bottom quartile of the 1970–2004 climatological distribution for those months. In contrast, August was a very active month with eight TCs, which is slightly above the 75th percentile of the distribution of seven; four of these reached TY intensity, and two became super-TYs (Saomai and Ioke). September and October had a normal level of TCs, with five and four TCs, respectively, equal to the median of the climatological distribution for those months. November and December had two TCs, corresponding to the 25th and 75th percentiles of the climatological distribution for those months, respectively. The cumulative distribution (Fig. 4.14b) shows a slightly below-normal season throughout the year.

The ACE Index (Bell et al. 2000) was slightly above the climatological median in 2006, in spite of the low number of TCs, because of the high number of intense TYs in 2006 (see Fig. 4.15a). The seven super-TYs contributed to 64% of the ACE of the 2006 season; the largest contribution was from the very long lasting super-TY Ioke, which provided 17% of 2006 ACE and had the 15th highest ACE per storm value (in the top one percentile) of the historical record. The 2006 ACE per month is shown in Fig. 4.15b compared with the 1970–2004 climatology. In the months of May and September, values of ACE were in the top quartile of the climatology, due to the occurrence of super-TYs Chanchu (May), Ioke (August–September), and Yagi (September), and TYs

Shansha and Xangsane (September).

The number of days with TCs that reached TS intensity or higher in 2006 was 132.25 (based on preliminary JTWC data), which was below the climatological median of 159 days, but slightly above the 25th percentile of the climatological distribution (128 days). There were 75.5 days with TYs in 2006, which was above the climatological median of 57.25 days, and very near the 75th percentile of the 1970–2004 distribution (76.4 days). There were 32.75 days with intense TYs (with sustained winds ≥ 96 kt) in the top quartile of the climatological distribution (75th percentile is 27.1 days). Figure 4.16 shows a scatterplot of the number of days with intense TYs and the Niño-3.4 index (Barnston et al. 1997) for July–October; note that for higher values of the Niño-3.4 index (El Niño years) there is a tendency for more days with intense TYs, as discussed in Camargo and Sobel (2005). Another typical characteristic of El Niño years is a tendency for long-lived TCs (Wang and Chan 2002; Camargo and Sobel 2005). In 2006, 7 of the 24 named TCs' lifetimes were longer than the median of the climatological distribution of 7.25 days. One super-TY, Ioke, had a very long lifetime of 16.25 days, which is in the top quartile of the climatological lifetime distribution. There were, however, many short-lived named TCs in 2006, nine of which had lifetimes in the bottom quartile of the climatological lifetime distribution.

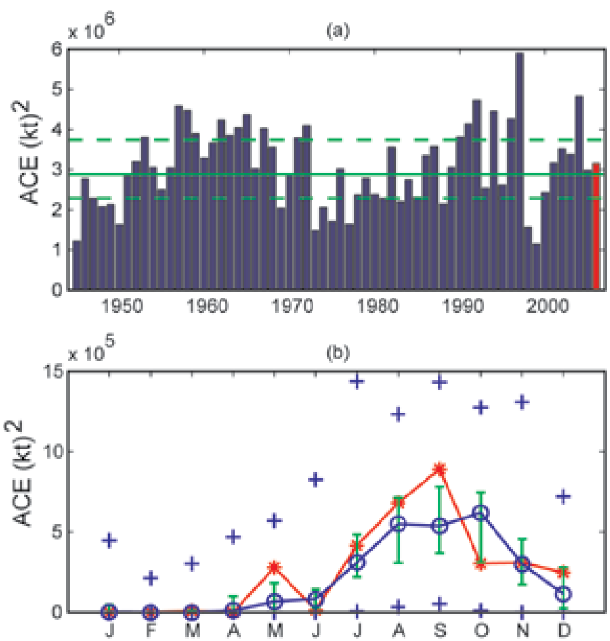

Fig. 4.15. (a) ACE Index (x 10^4 kt^2) per year in the western North Pacific for the years 1945–2006. The solid green line indicates the median for the 1970–2004 climatology, and the dashed green lines show the 25th and 75th percentiles. (b) ACE Index per month in 2006 (red line) and the median in the years 1970–2004 (blue line), where the green error bars indicate the 25th and 75th percentiles. In the cases of no error bars, the upper and/or lower percentiles coincide with the median. The blue plus signs (+) denote the maximum and minimum values during the period 1945–2006.

A well-known influence of ENSO on western North Pacific TC activity is a southeast (northwest) shift of the mean genesis location within the region in El Niño (La Niña) years (e.g., Chan 1985; Chia and Ropelewski 2002). In 2006, the mean average genesis position of the NSs was 13.9°N, 139.8°E, which is slightly northwest of the climatological mean genesis position (12.8°N, 143.2°E; standard deviations: 1.9° latitude, 6.6° longitude). Therefore, the typical southeast shift of genesis in El Niño years did not occur in 2006. However, the mean track position of NSs was 18.8°N, 131.2°E, which is slightly east of the climatological mean position (19.0°N, 134.1°E), largely due to the contribution of the long-lived Ioke, with a track starting in the central Pacific.

The 2006 El Niño started late and was not very strong, attaining moderate strength in November after the peak TY season. Therefore, its influence on the TY season was not typical. In Fig. 4.17a the SST anomalies in the months of July–October (when the peak TY season occurs) are shown with a slightly

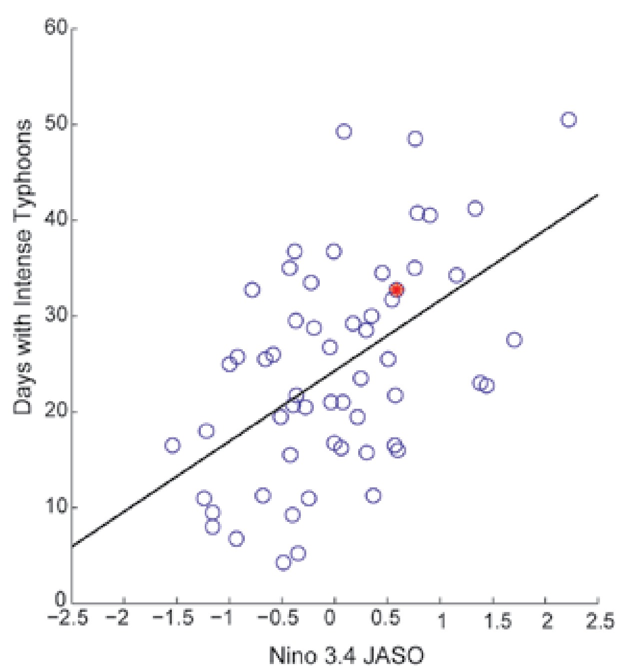

Fig. 4.16. Scatterplot of number of days with intense typhoons and Niño-3.4 index (°C) for JASO in the period 1950–2006; the black line is the linear regression, the number of intense typhoons for 2006 is marked in red (r = 0.52).

positive SST anomaly in the central Pacific region. As shown in Chan and Liu (2004), the western North Pacific TY activity does not have a relationship with local SSTs. However, there is a relationship with large-scale dynamics associated with El Niño events, such as the extension of the low-level anomalous westerlies from the monsoon trough. In strong and typical moderate El Niño events, the anomalous westerlies extended throughout the western North Pacific (see, e.g., Camargo et al. 2007). In 2006, however, the anomalous westerlies were present just west of 150°E (Fig. 4.17b). There was no TC genesis in 2006 east of 150°E, with exception of TYs with more subtropical genesis locations and Ioke, with a genesis location in the central Pacific (Chan 2007).

Some interesting events occurred in the 2006 TY season. Super-TY Chanchu (8–18 May) attained that status in the South China Sea, a rare occurrence, with only two other TCs reaching that intensity in the area before: Ryan (1995) and Sally (1996). Chanchu was also the earliest system to become a super-TY in the South China Sea (Padgett 2007). Super-TY Saomai (4–14 August) made landfall in eastern China, and was the strongest TY to make landfall in China in the modern record (Padgett 2007). Super-TY Saomai, TS Bopha (6–10 August), and TY Maria (5–9 August) coexisted in the western North Pacific, contributing to a very busy month of August in the basin. Tropical storms Wukong (12–19 August) and Sonamu (13–16 August) formed in a large monsoon gyre. The monsoon gyre is an episodic event, occurring approximately once a year and lasting from two to three weeks, and often TCs are produced in the eastern periphery of the gyre (Lander 1994). Wukong and Saomai underwent a binary interaction, and the stronger Wukong absorbed Sonamu, similar to the case described in Lander (1995). The strongest TC in 2006 was super-TY Yagi, which did not affect any major land areas.

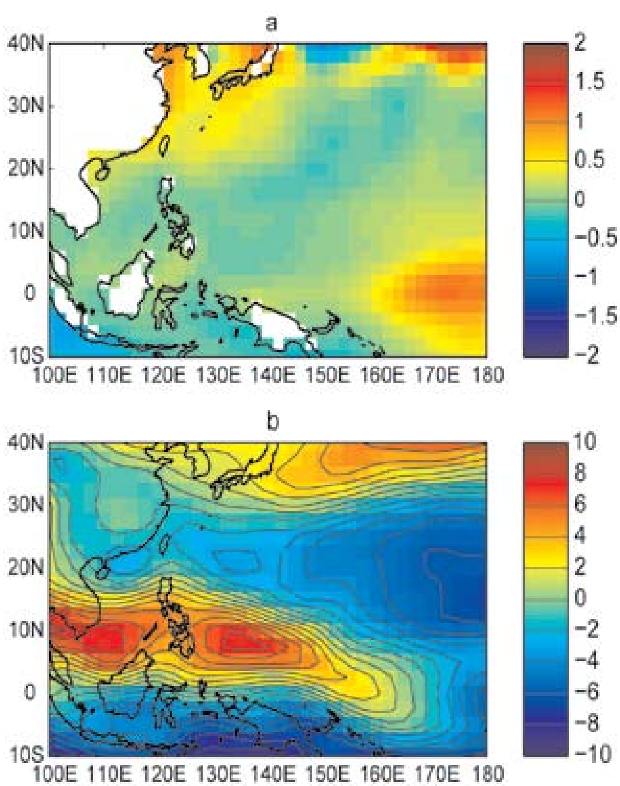

Fig. 4.17. (a) SST anomalies (°C) from July to October of 2006. (b) Anomalous 850-hPa zonal winds (m s^{-1}) from July to October of 2006.

The 2006 western North Pacific TY season was responsible for many fatalities and economic losses, primarily in the Philippines and China, with eight and four landfalls, respectively. Other countries affected by TCs in the 2006 season were Vietnam, Taiwan, Japan, and South Korea. Bilis (8–15 July), though only reaching TS intensity, was responsible for 672 deaths in China and over $2.5 billion (USD) in economic losses due to very heavy rain, flooding, and landslides. Bilis was soon followed by TYs Kaemi (8–16 July) and Prapiroon (28 July–5 August), which also struck China and caused more economic losses and resulted in over 100 deaths. Typhoon Xangsane (25 September–2 October) had significant impacts in the Philippines, where strong winds and heavy rainfall led to numerous mudflows and the death of over 200 people, before striking Vietnam where 71 deaths were reported. Typhoons Cimaron (26 October–6 November), Chebi (8–14 November), Durian (24 November–5 December), and Utor (7–14 December) all made landfall in the Philippines. Typhoon Durian was responsible for at least 720 deaths resulting from mudslides of volcanic ash, which covered houses in a large portion of Legazpi City.

5) Indian Ocean basins—K. L. Gleason

(i) North Indian Ocean (NIO)

The NIO TC season extends from April to December, with two peaks in activity during May–June and again in November when the monsoon trough is climatologically positioned over tropical waters in the basin. Tropical cyclones in the NIO basin develop in the Bay of Bengal and the Arabian Sea typically between 8° and 15°N latitude and are usually short lived and weak, quickly moving into the subcontinent.

[5] The Bangladesh supercyclone of 1970 produced perhaps the greatest human fatality toll on record from a TC, where at least 300,000 people died, primarily from the associated storm surge in the low-lying deltas (Holland 1993).

However, strong and "severe cyclonic storms,"[5] as illustrated by Neumann et al. (1993), can develop with winds greater than 130 kt.

Using reliable records from 1981 to 2000, a mean of nearly five NSs (sustained winds ≥ 34 kt), 1.6 TCs (sustained winds ≥ 64 kt), and one MTC (sustained winds ≥ 96 kt) form each year in the NIO. The 2006 TC season was near average with five NSs, one TC, and one MTC forming from January to December (Fig. 4.18a). Regarding the overall level of TC activity, the estimated ACE Index for the NIO basin in 2006 was nearly 14×10^4 kt^2, which was less than the 1981–2000 mean of 17×10^4 kt^2 (Fig. 4.18b). In fact, the annual ACE values in the NIO over the past seven years have all been below average, indicating a period of decreased activity. This most recent period of below-normal activity followed four active TC seasons with above-average ACE values during the late 1990s (Fig. 4.18b).

Severe TC Mala was the only TY-strength storm to form during 2006. Mala developed off the western tip of Sumatra on 24 April and tracked northwest into the central Bay of Bengal. By 25 April, Mala had intensified into the equivalent of a category 1 TC on the Saffir-Simpson scale and began to accelerate to the northeast. TC Mala continued to intensify over the next several days and with winds speeds over 185 km h^{-1} (115 kt) on 28 April, attained peak intensity, and became the first major cyclone in the NIO since 2001. Shortly after attaining peak intensity, MCYC Mala weakened somewhat before making landfall over Myanmar on 29 April. The hardest hit area was near Yangon, with more than 100 buildings and numerous power lines damaged by the strong winds. Extreme storm surge and large waves caused severe structural damage. Heavy rainfall associated with Mala also caused flooding, which resulted in at least 22 fatalities in this region.

(ii) South Indian Ocean

The TC season in the SIO is typically active from December through April and officially extends from July to June, spanning across parts of two calendar years. The SIO basin extends south of the equator from the African coastline to 105°E, although most cyclones develop south of 10°S latitude. Cyclones in the SIO that remain east of 105°E are included in the Australian summary (see section 4c7). The vast majority of SIO landfalling TCs impact Madagascar, Mozambique, and the Mascarene Islands, including Mauritius. Due to a lack of historical record keeping by individual countries and no centralized monitoring agency, the SIO is probably the least understood of all TC basins (Atkinson 1971; Neumann et al. 1993). As a result of the disparate nature of the data in this region, the SIO historical statistics presented are incomplete, especially prior to the late-1970s.

Using reliable data from 1981 to 2000, the SIO averages 11.9 NSs, 6.2 TCs, and 2.8 MTCs each year. During the 2005/06 season (July 2005–June 2006), the SIO TC occurrences were below average with 9 NSs, 3 TCs, and 3 MTs (Fig. 4.19a). The estimated ACE Index for the SIO during 2005/06 was 55×10^4 kt^2, which is slightly more than half of the 1981–2000 average of 107×10^4 kt^2 (Fig. 4.19b). The SIO ACE Index values over the last three years were below average and the 2006 ACE value was the fifth lowest value since 1980. During the 2005/06 season, the strongest TC in the SIO was MTC Carina with 130-kt sustained winds.

The first major TC in the southeast Indian Ocean

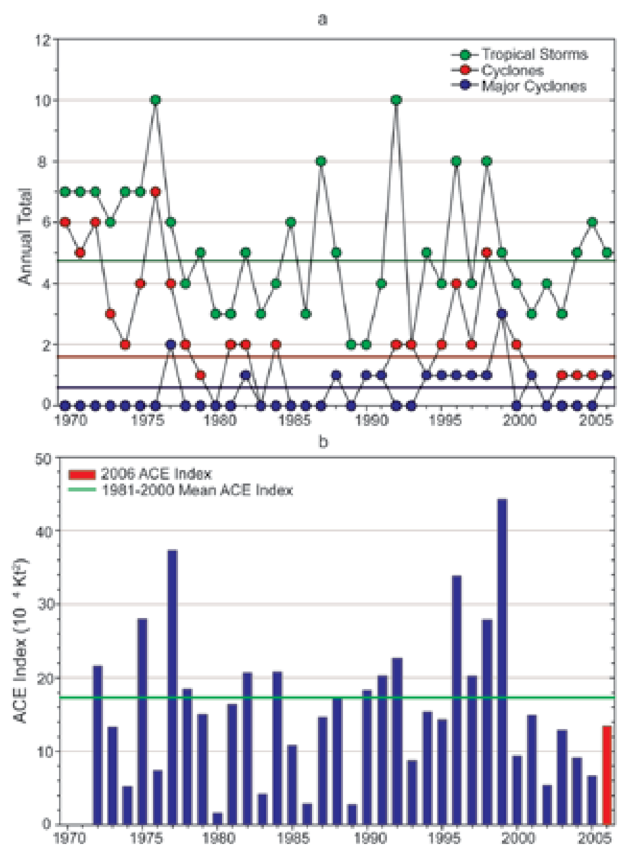

Fig. 4.18. Annual tropical cyclone statistics for the North Indian Ocean over the period of 1970–2006: (a) number of tropical storms, cyclones, and major cyclones, and (b) the estimated annual ACE Index (x 10^4 kt^2) for all tropical cyclones during which they were at least tropical storm or greater intensities (Bell et al. 2000). The 1981–2000 base period means are included in both (a) and (b). Note that the ACE Index is estimated due to a lack of consistent 6-h sustained winds for every storm.

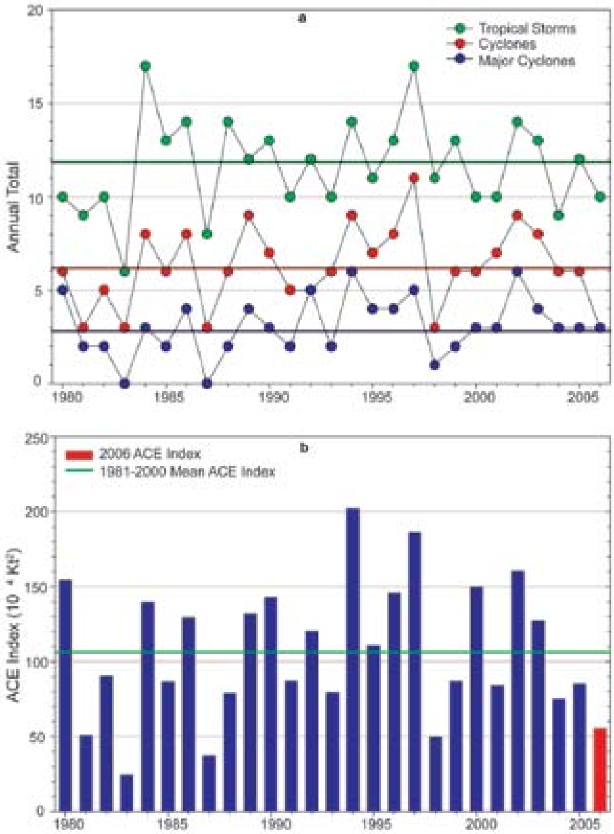

Fig. 4.19. Same as Fig. 4.18, but for TCs in the South Indian Ocean over the period 1980–2006.

formed east of 90° during mid-November 2005 and was named Bertie. This storm gradually strengthened and was classified as a severe TC on 21 November. By the 23 November, Bertie entered the southwest Indian Ocean and was renamed Alvin. That same day, Bertie/Alvin reached peak intensity of 115 kt, which is the equivalent of a weak category 4 TC. The storm weakened shortly after attaining peak intensity and dissipated by the end of the month.

TC Boloetse formed off the eastern coast of Madagascar during late January 2006. Boloetse intensified into a tropical storm with sustained winds of 50 kt before making landfall near the village of Mananjary on 29 January. After crossing the island, Boloetse remerged and reorganized in the Mozambique Channel. Gaining intensity, this storm reached a peak intensity of 100 kt in early February, the equivalent of a category 3 cyclone on the Saffir–Simpson scale. Eventually, CYC Boloetse tracked southwest of Madagascar before it transitioned to being extratropical. Boloetse was the only TC that made landfall during the 2005/06 season.

The most intense TC in the SIO during the 2005/06 season was MTC Carina, which attained peak sustained winds of 130 kt. Carina developed in late February 2006 southeast of Diego Garcia in the central Indian Ocean and quickly strengthened into a moderate tropical storm. While remaining over open waters and among favorable conditions for development, Carina deepened and became a MTC as it moved to the southwest. On 28 February, MTC Carina neared category 5 strength on the Saffir–Simpson scale as it reached a peak intensity of 130 kt. Shortly after attaining this intensity, the storm entered an unfavorable environment with high wind shear and began to dissipate.

6) Southwest Pacific basin—M. J. Salinger and S. M. Burgess

The southwest Pacific experienced nine occurrences (east of 150°E) of TCs during 2006, equal to the average number normally expected for the region in a year (Fig. 4.20). There was also one occurrence that originated adjacent to the region, just west of 150°E. Many of the seasons' occurrences affected the region west of the date line, with the highest frequency of occurrences in the Coral Sea since at least 1999/2000 (Fig. 4.21). This was consistent with weak La Niña conditions in early 2006. There was an even spread of TCs throughout the period from January to March, and the most severe portion of the season was in April. Above-average SSTs combined with enhanced convection over the Coral Sea, and assisted in the development of TCs in that area of the basin. Seven of the southwest Pacific basin TCs (71%) reached H strength (sustained wind speeds of at least 118 km h^{-1}), and three major hurricane strength (sustained wind speeds of at least 168 km h^{-1}).

TC Tam was the first TC of the season, which occurred north of Fiji on 12 January, and tracked toward Tonga on 13 February, to pass west of Niue, with gale force winds. Urmil occurred on 15 January, and tracked well south of Niue with maximum sustained winds of 85 km h^{-1}. TC Jim occurred next, with sustained wind speeds of at least

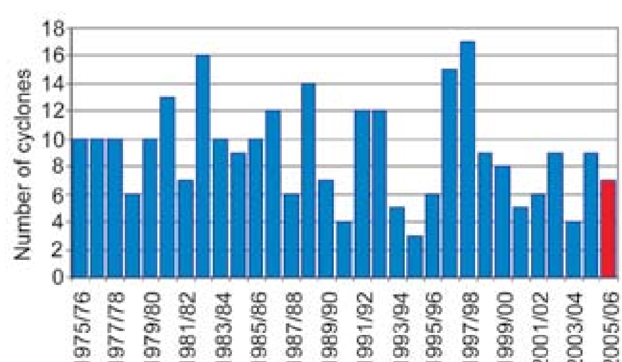

Fig. 4.20. The number of southwest Pacific TCs for the 2005/06 season (solid red bar) compared to frequencies during the past 30 yr. For the 2006 calendar year there were nine.

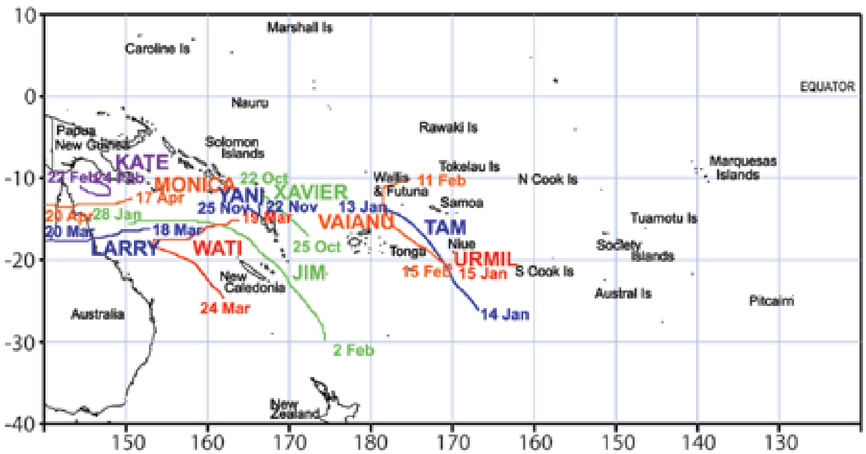

Fig. 4.21. Southwest Pacific TC tracks for the 2005/06 season (including Monica).

155 km h^{-1} (hurricane force). Jim was located in the Coral Sea on 28 January, and later tracked southeast to pass between New Caledonia and Vanuatu. A mean speed of 154 km h^{-1} (H force) was noted at Pekoa in northern Vanuatu on 31 January. TC Vaianu from 11 to 15 February produced sustained wind speeds of 140 km h^{-1}. Vaianu affected open waters near the Wallis and Futuna and Tongan Islands. TC Kate occurred from 24 to 25 February with sustained wind speeds of 90 km h^{-1}. Kate was fairly localized, occurring over the Coral Sea south of Papua New Guinea. The TCs in March were Larry (18–20 March) (see section 7) and Wati (19–24 March). TC Wati affected the open waters west of Vanuatu and New Caledonia, with estimated maximum wind speeds of 150 km h^{-1}. TC Monica (see section 7) was the last to affect the southwest Pacific in mid-April.

The 2006/07 season commenced unusually early, consistent with El Niño conditions later in the year, on 22 October. While not part of the TC season described in this section, we note that two named TCs for the 2006/07 season occurred prior to the end of calendar year 2006. TC Xavier occurred from 22 to 25 October, with estimated maximum sustained wind speeds reaching 215 km h^{-1}, and TC Yani from 22 to 25 November had estimated maximum sustained wind speeds of 120 km h^{-1}. Both occurred between the Solomon Islands and Fiji.

7) Australian basin—A. B. Watkins

Weak La Niña–like conditions in the equatorial Pacific Ocean and warmer SSTs off the northern and eastern coasts of Australia contributed to the slightly above average 2005/06 TC season. A total of 12 TCs occurred in the Australian region between 105° and 160°E, 2 more than the long-term average of approximately 10. However, 3 of these 12 reached category 5 on the Australian scale, with TC Larry being the strongest cyclone to make landfall in Queensland since 1918, and TC Monica the strongest TC ever observed in the Northern Territory region. In the western Australian/Indian Ocean sector, seven TCs were recorded as follows: Bertie (category 4), Clare (3), Daryl (2), Emma (1), Floyd (4), Glenda (5), and Hubert (2); and in the Queensland/Pacific sector, Jim (3), Kate (2), Larry (5), and Wati (3); and in the Queensland and Northern Territory region: Monica (5).

For more information on the category 5 TCs in the Australian basin (Larry, Monica, and Glenda), please see the "An Australian Season of Extremes" sidebar.

d. *Intertropical convergence zones*

1) Pacific ITCZ—A. B. Mullan

Three convergence zones can be identified in the Pacific: the ITCZ in the NH at around 5°–10°N; its Southern Hemisphere counterpart, denoted separately here as SITCZ; and the SPCZ, which extends diagonally from around the Solomon Islands (10°S, 160°E) to near 30°S, 140°W. The SITCZ only occasionally extends eastward of about 160°W, and west of this point often merges with the SPCZ, making it difficult to separate the two features in the southwestern Pacific.

The year 2006 saw a weak La Niña event end in the first few months, followed by the development of a moderate El Niño by mid-September that peaked at the end of the year. La Niña conditions in March–April are known to promote the appearance of a "double ITCZ" (Lietzke et al. 2001; Zhang 2001), and Fig. 4.22 shows a striking example of this. The SITCZ convection for March 2006 is continuous from 85°W to west of the date line, is stronger than a rather broken northern ITCZ, and shows a clear separation from a weak SPCZ farther south. Similar convection patterns are evident in TRMM rainfall data for March 1999 and 2000 (also La Niña periods), although in those years the separation from the SPCZ is not as marked. As noted by Gu et al. (2005), there appears to be some competition between the two ITCZs as measured by rainfall, and the northern ITCZ is

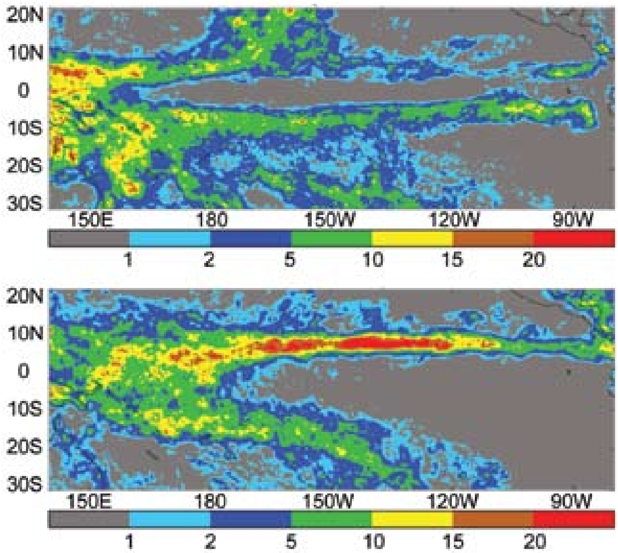

FIG. 4.22. Average rainfall rate (mm day^{-1}) from TRMM 0.25° analysis for months of March (upper panel) and December (lower panel) 2006. Contours at uneven spacing of 1, 2, 5, 10, 15, and 20 mm day^{-1}.

weaker at this time than the prominent SITCZ.

A more typical two–convergence zone pattern is seen in the rainfall rate for December 2006 (Fig. 4.22, lower panel). A prominent ITCZ is particularly active east of the date line, and the SPCZ is bowed northward near 150°W, both features characteristic of El Niño conditions. For the year as a whole, the TRMM rainfall data suggest that rainfall was close to the 1999–2005 average over much of the tropical Pacific, with the exception of enhanced convection in the SITCZ region. (See section 6hiii for further information on the SPCZ.)

The seasonal progression of convection through 2006 is shown in Fig. 4.23, where area-averaged rainfall rates have been calculated for the following three convergence zone regions: ITCZ (0°–15°N, 150°E–90°), SITCZ (0°–10°S, 150°–80°W); and SPCZ (0°–30°S, 150°E–90°). These boundaries are chosen after examination of the data to avoid the complications of the merging ITCZ and SPCZ in the far western tropical Pacific, and the orographic rainfall over Central America near 80°W. The SITCZ region is limited to the east of 150°W, even though at rare times (Fig. 4.22) the southern ITCZ is distinct from the SPCZ west of this point. In calculating the SPCZ area-averaged rainfall, the rainfall within the SITCZ part of the domain is set to zero. To place all three quite different domains on a more equal footing, the monthly area averages are normalized by the 1999–2005 annual average for each region. Thus, Fig. 4.23 shows both the climatological annual cycle (dotted lines) and the monthly progression

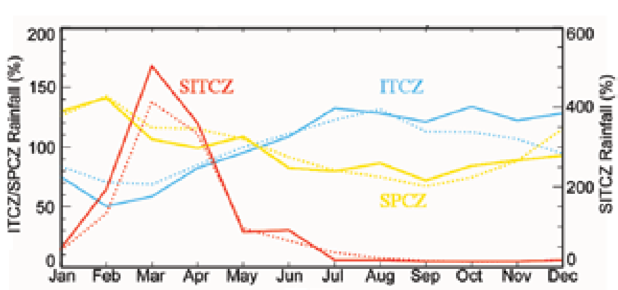

FIG. 4.23. Area-averaged TRMM rainfall for the three convergence zone regions: ITCZ, 0°–15°N, 150°E–90°; SITCZ, 0°–10°S, 150°W–80°W; SPCZ, 0°–30°S, 150°E–90° (but excluding the SITCZ region). Monthly values are expressed as percentages of the 1999–2005 annual average. Solid lines show 2006 variation, and dotted lines the average variation over 1999–2005. Note the different ordinate scale (right-hand axis) for SITCZ.

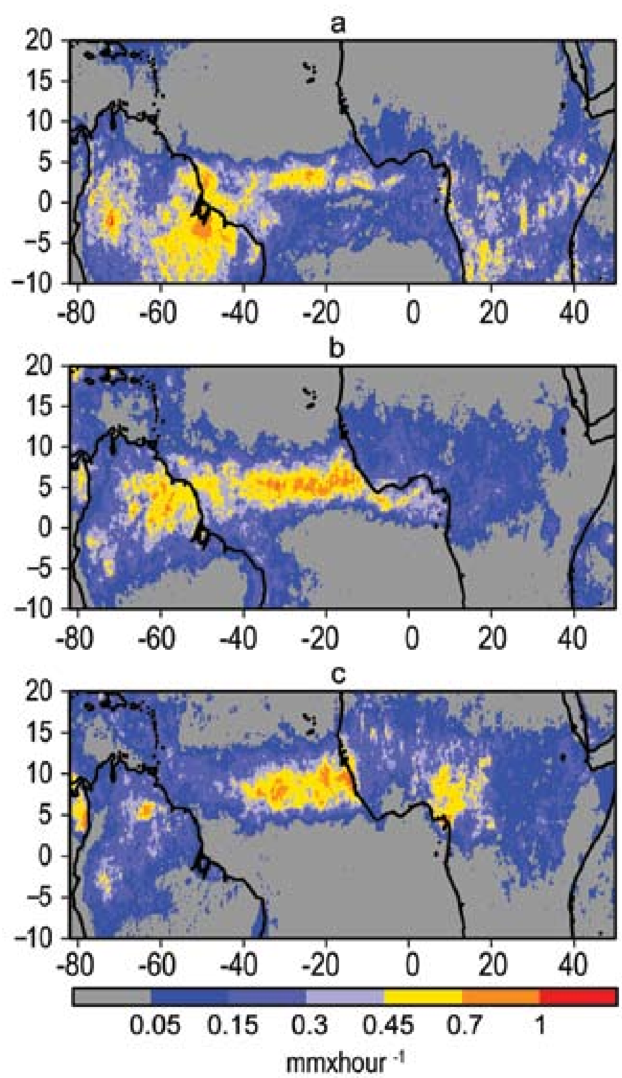

FIG. 4.24. Average rainfall rate (mm h^{-1}) from high-resolution (0.25° latitude × 0.25° longitude) TRMM analysis for (a) April, (b) June, and (c) August 2006.

AN AUSTRALIAN SEASON OF EXTREMES: Yes, We Have No Bananas—

A. B. Watkins, H. J. Diamond, and B. C. Trewin

The 2005/06 TC season in Australia was only slightly above average when judged by TC frequency. When viewed in terms of intensity, it ranks as one of Australia's most extreme TC seasons on record. Of the 12 TCs of the season, 3 were Australian category 5, with 1 being the strongest to hit Queensland in nearly 90 years, and another being the strongest TC ever reported off the Northern Territory coast and one of the strongest ever in the Australian region. Although only one TC made landfall as category 5, each severe TC had impacts upon a different state or territory within Australia.

If you lived in Australia and craved a banana with your cereal, banana chips with lunch, or the occasional banana daiquiri, then 2006 was just not your year. When TC Larry blasted across the northern Queensland coast, it devastated the Australian banana crop, drastically limiting supply and raising prices Australia-wide by 400%–500%, arguably triggering a small rise in Australia's inflation rate.

TC Larry (Fig. 4.25) crossed the north Queensland coast near Innisfail on the morning of 20 March 2006. Larry reached category 5 intensity shortly before reaching the coast, but crossed as category 4. This was supported by a wind gust of 293.7 km h^{-1} recorded on the eastern (leeward) slope of Mount Bellenden Ker at an elevation of approximately 1450 m, although by an instrument on a tower at nonstandard height. Worst affected was the town of Silkwood, where 99% of the houses suffered cyclone damage. In total, the immediate impact of the cyclone caused over $350 million Australian dollars of insured losses.

TC Larry destroyed between 80%–90% of the total Australian banana crop (Fig. 4.26). In addition to limiting supply, it served to synchronize the crop, which had been staggered through the year to ensure a constant supply and stable prices.

The second record TC of the season was severe TC Monica, which followed a very long track (Fig. 4.27) from the Coral Sea east of Queensland, crossing the Cape York Peninsula and then intensifying along the northern coast of the Northern Territory before making landfall north of Jabiru on 24 April. During its passage along the Northern Territory coast, it intensified into a category 5 system, and one of the most powerful cyclones witnessed in the Australian region and the strongest cyclone ever observed in the Northern Territory. Estimated wind speeds were in excess of 350 km h^{-1} on both 23 and 24 April. There was evidence of a 5–6-m storm surge zone in Junction Bay.

Severe TC Glenda was a small but intense system that developed rapidly after moving off the northwest coast of Western Australia near Kimberley. Glenda reached category 5 intensity with estimated wind gusts to 300 km h^{-1}, but weakened as it approached the Pilbara coast. It weakened before finally crossing the coast near Onslow on 30 March as a marginal category 3.

The 2005/06 TC season in Australia was clearly one of its most intense on record. Fortunately, the strongest storms either missed heavily populated areas or reduced in intensity at just the right time, and hence, damage to property and loss of life was kept relatively low. However, in Queensland at least, the effect of a severe TC upon agriculture was devastating; an impact ultimately felt across the country.

Fig. 4.25. Tropical Cyclone Larry viewed just after landfall, 0730 Australian EST 20 Mar 2006.

Fig. 4.26. Damage to the banana crop as a result of Tropical Cyclone Larry.

Fig. 4.27. Track of TC Monica, the strongest TC ever recorded in the Northern Territory region.

during 2006 for comparison. Note that although the TRMM rainfall dataset begins in 1998, the long-term averages are taken from 1999 because extreme El Niño conditions in the first few months of 1998 distort the rainfall climatology in the SITCZ region.

Rainfall in the ITCZ is higher in the second 6 months of the year, and this climatological pattern was accentuated during 2006. Rainfall was lower than normal, particularly in February, and higher than normal in October through December 2006. This transition was also apparent in island rainfall records for the year. The islands of Micronesia in the western Pacific, which enter their dry season at the start of the calendar year, were very dry in some parts (e.g., the northern Marshall Islands) in the first quarter of 2006. South of the equator, rainfall in specific island groups was affected by the ENSO modulation of the SPCZ. The SPCZ was farther south than usual from January through May, as expected with La Niña, and farther north than usual in at least some months at the end of 2006 (e.g., December). However, in the area average of the SPCZ region plotted in Fig. 4.23, these local precipitation fluctuations average out and there is no marked pattern of precipitation anomalies through the year. As noted above, precipitation in the SITCZ region, which occurs mainly from February through April, was enhanced during 2006.

2) Atlantic ITCZ—A. B. Pezza and C. A. S. Coelho

The Atlantic ITCZ is a narrow but well-organized convective region that oscillates between several degrees north of the equator during July–November and only a few degrees south of the equator in January–May (Waliser and Gautier 1993). The ITCZ is active all year-round, demarcating the transition from the southeasterly to the northeasterly Atlantic trade winds. A zonally oriented cloud band is usually observed over the Atlantic Ocean basin extending from the northeast coast of South America to the northwest coast of Africa. Convective activity with high rainfall rates well inland is generally triggered by the nearby passage of the ITCZ as observed over northern Amazon in 2006 (Fig. 4.24).

The positioning of the ITCZ modulates the rainy season of northern/northeastern South America and northwestern Africa. Some regions experience a bimodal monthly rainfall distribution with two peaks—one when the ITCZ is moving southward and the other when it is moving back northward. Its seasonal migration and high asymmetry are primarily driven by land–sea temperature contrast, low-level winds, moisture convergence, and the meridional SST gradient between the North and the South Atlantic (Nobre and Shukla 1996). Large-scale dynamics given by Kelvin wave propagation affecting the Walker circulation can also drive the ITCZ's interannual variability, because ENSO is one of the relevant mechanisms of seasonal influences (Münnich and Neelin 2005).

High-resolution TRMM data indicate that during 2006 the ITCZ reached its southernmost position in April (2.5°S) and its northernmost position in August and September (10°N), and was to the north of its monthly climatological mean position during a number of months, particularly during the second half of the year. As a result, most of the tropical South Atlantic presented less rainfall in 2006 than the 1998–2005 annual mean value. However, the 2006 ITCZ's annual mean position appears close to its climatological annual mean due to a high variability, with outbursts of southward displacement from late austral summer to early austral winter. TRMM also shows a double ITCZ (Liu and Xie 2002) during April, with a primary band of convective clouds around 3°N across the entire equatorial Atlantic, and a secondary band of clouds around 2.5°S (Fig. 4.24).

April featured the interaction and organization of the secondary ITCZ branch with continental convection over northern Brazil, resulting in a wider ITCZ to the west of 30°W. This interaction over northern Brazil was also noted in May and June (Fig. 4.24), decaying in July. The ITCZ became less active from September to December, with little rainfall observed in September around 7.5°N in the central North Atlantic and near the African coast. August was the most active month for the period from July to December, when some areas near the African coast experienced high rainfall rates (Fig. 4.24). Interaction with western Africa rain was irregular during the year, with areas of positive and negative precipitation anomalies observed over the western tip of the continent. The onset of a weak El Niño event in the Pacific during mid-2006 contributed to keeping most of the ITCZ convective activity to the north of the equator for the remainder of the year, with annual rainfall below average over most tropical South Atlantic and above average over the tropical North Atlantic.

5. THE POLES—F. Fetterer, Ed.

a. *Arctic*—J. Richter-Menge, J. Overland, A. Proshutinsky, V. Romanovsky, R. Armstrong, J. Morison, S. Nghiem, N. Oberman, D. Perovich, I. Rigor, L. Bengtsson, R. Przybylak, A. Shiklomanov, D. Walker, and J. Walsh

1) Overview

The permanent presence of sea ice, ice sheets, and